Gasification of Biomass in an Updraft Fixed Bed Reactor: Effect of Viscous Models

F. J. Alarcón-Gaete and J. C. Elicer-Cortés*

Departamento De Ingeniería Mecánica, Universidad De Chile, Beauchef 851, Santiago, Chile

Abstract: A numerical study to investigate the influence of viscous models in the biomass gasification in an updraft fixed bed reactor is presented. The unsteady simulations were performed using finite volume method of ANSYS Fluent. A two-dimensional axisymmetric transient model was used to simulate the biomass gasification process. The model is based on the Euler-Euler multiphase formulation. The reactive gas-solid flow considers both homogeneous and heterogeneous reactions (drying, pyrolysis, combustion and gasification). Source terms and chemical kinetics are incorporated into the code using user-defined functions programmed in C. Results are validated with experimental data available in the literature for gasification in a continuous reactor. Temperatures and mole fractions of CO, CO_2, CH_4, Tar, and H_2 at the reactor exit are in good agreement with the experimental measurements. Laminar model is agreed with experimental data for net calorific value, however, discrepancies are observed when the $k-\varepsilon$ mixture model is used. This work provides a methodology for studying gasification in fixed beds using a commercial CFD code which can be used in gasifier design, analysis, and optimization.

Keywords: CFD, euler-euler approach, multiphase flow, fixed bed, updraft gasifiers, biomass fuel.

1. INTRODUCTION

Updraft fixed-bed gasifiers are the most widely used in thermal applications below 10 MW. The process has a high thermal efficiency because the gas leaves the reactor at relatively low temperatures. The carbonaceous particles (e.g., coal or biomass), are fed at the top of the reactor and flow slowly to the bottom, from where the residue is extracted. The gasifying agent, normally air and steam, is injected through the distributor at the bottom. In the downward motion, the solid undergoes the drying, pyrolysis, gasification, and combustion processes. The main product desired in the gasification is the synthesis gas (syngas), which is a gaseous mixture, composed mainly of carbon monoxide, carbon dioxide and hydrogen.

Computational fluid dynamics (CFD) simulation is an essential tool for design, analysis and optimization in all engineering fields. This technique allows the analysis of the data in several configurations and scales using a lower number of experiments. The large number of studies available in the literature proves the analysis tool utility. Experimental studies are also needed to establish the validity of a given computational model. In relation to numerical simulations of solid fuels (coal, biomass) gasification process in entrained flow, fixed bed, fluidized bed and spouted bed reactors, research has focused primarily on developing computer codes based on equilibrium and non-equilibrium chemical models, artificial neural networks, Euler-Lagrange model sand Euler-Euler models [1-11].

One-dimensional (1D) mathematical models are widely used to study the process in updraft and downdraft reactors [12-18]. These models are based on solving the governing equations derived from the conservation laws (mass, momentum and energy) for both gas and solid phases.

In recent years, two-dimensional (2D) multiphase models based on the Euler-Euler approach or also called two-fluid model (TFM) have been proposed [7, 19-21]. In these models, solid phase rheology is described by equations of the kinetic theory of granular flow (KTGF).

This paper reports a multiphase computational fluid dynamic study of a fixed bed wood gasifier. The simulations use the Eulerian-Eulerian framework within the commercial CFD code FLUENT. The model consists of several sub routines written in C, which calculate specific aspects of the phenomenon under study, not included in ANSYS FLUENT, such as chemical kinetics, source terms and additional boundary conditions.

2. GASIFICATION MECHANISM AND KINETIC MODEL

2.1. Reaction Mechanism

2.1.1. Drying

Drying is the first process that takes place during the heating of solid fuel, and its importance lies in the

*Address correspondence to this author at the Departamento de Ingeniería Mecánica, Universidad de Chile, Beauchef 851, Santiago, Chile;
Tel: (56) 22978 45 42; Fax: (56) 22698 84 53; E-mail: jelicer@ing.uchile.cl

E-ISSN: 2409-5826/16

influence it has on the temperature fields [22]. The drying process can be represented by the following heterogeneous reaction:

$$H_2O(l) \rightarrow H_2O(g) \quad (R_1)$$

2.2.2. Pyrolysis

Pyrolysis is a very complex process involving many reactions, including heat and mass transfer that result in a release of a mixture of organic and inorganic gases from the surrounding particles. This release is due to the increase in temperature of the particles. Because of this complexity, devolatilization of carbonaceous fuels is one of the most researched topics today [23].

During the biomass pyrolysis are released mainly:

- Light hydrocarbon and non-hydrocarbons gases, such as CH_4, C_2H_6, H_2, CO, CO_2, etc.
- Tar ($C_mH_nO_l$). It consists of heavy organic and inorganic molecules escaping from the solid as gases
- Char (CH_xO_y (s))

The pyrolysis process can be represented by the following heterogeneous reaction:

$$W \rightarrow \beta_{CH_xO_y(s)}\mathrm{CH_xO_y}(s) + \beta_{CO_2}\mathrm{CO_2} + \beta_{H_2O}\mathrm{H_2O} + \\ + \beta_{C_mH_nO_l}\mathrm{C_mH_nO_l} + \beta_{CO}\mathrm{CO} + \beta_{H_2}\mathrm{H_2} + \beta_{CH_4}\mathrm{CH_4} \quad (R_{21})$$

where coefficients are determined from a mass and energy balance [24].

2.2.3. Tar Cracking

The tars released during pyrolysis often undergo a decomposition that produces secondary gases. The decomposition of the tar can be modeled by means of a one-step overall reaction.

$$\mathrm{Tar\ (C_mH_nO_l)} \rightarrow \gamma_{CO_2}\mathrm{CO_2} + \gamma_{H_2O}\mathrm{H_2O} \\ + \gamma_{CO}\mathrm{CO} + \gamma_{H_2}\mathrm{H_2} + \gamma_{CH_4}\mathrm{CH_4} \quad (R_{22})$$

Stoichiometric coefficients, γ_i, can be found in the literature for the case of biomass [25, 26].

2.2.4. Combustion and Gasification of Char

The oxidation or combustion of char is one of the chemical reactions that take place during the gasification process, providing practically all the thermal energy needed to sustain endothermic reactions. In addition to combustion of char, the oxygen supplied reacts with fuel species forming CO_2 and H_2O. The gasification reactions (Eqs. R_{32}, R_{33} and R_{34}) release combustible gases such as H_2, CO, and CH_4. The gasification process takes place in the conditions of air (or oxygen) deficit, thus maintaining reducing conditions. The air/fuel ratio, together with the reaction temperature, determines the composition of the gas. In this way biomass is converted into synthesis gas (syngas). The reactions considered in this study include $\mathrm{CH_xO_y}(s) - \mathrm{O_2}$, $\mathrm{CH_xO_y}(s) - \mathrm{H_2O}$, $\mathrm{CH_xO_y}(s) - \mathrm{CO_2}$ and $\mathrm{CH_xO_y}(s) - \mathrm{H_2}$ as shown below.

$$\mathrm{CH_xO_y}(s) + z\mathrm{O_2} \rightarrow \left(2 - 2z - y + \frac{x}{2}\right) \\ \mathrm{CO} + \left(2z + y - \frac{x}{2} - 1\right)\mathrm{CO_2} + \frac{x}{2}\mathrm{H_2O} \quad (R_{31})$$

$$\mathrm{CH_xO_y}(s) + (1-y)\mathrm{H_2O} \rightarrow \mathrm{CO} + \left(1 - y + \frac{x}{2}\right)\mathrm{H_2} \quad (R_{32})$$

$$\mathrm{CH_xO_y}(s) + \mathrm{CO_2} \rightarrow 2\mathrm{CO} + y\mathrm{H_2O} + \left(\frac{x}{2} - y\right)\mathrm{H_2} \quad (R_{33})$$

$$\mathrm{CH_xO_y}(s) + \left(2 - \frac{x}{2} + y\right)\mathrm{H_2} \rightarrow \mathrm{CH_4} + y\mathrm{H_2O} \quad (R_{34})$$

The z coefficient is determined from the ratio $CO/CO_2 = 2500\exp(-6240/T_1)$.

2.2.5. Homogeneous Gas Phase Reactions

Since the gas-phase syngas combustion reaction taking place in this study is for syngas with relatively low concentration of oxygen, a simplified reaction mechanism for the current system has been used based on other studies [7, 12], as shown in Eqs. R_{41}, R_{42} and R_{43}. The main reaction of our mechanism is the water-gas shift reaction which is a well-known step for upgrading carbon monoxide to hydrogen in the production of syngas.

$$\mathrm{H_2} + \frac{1}{2}\mathrm{O_2} \rightarrow \mathrm{H_2O} \quad (R_{41})$$

$$\mathrm{CO} + \frac{1}{2}\mathrm{O_2} \rightarrow \mathrm{CO_2} \quad (R_{42})$$

$$\mathrm{CH_4} + \frac{3}{2}\mathrm{O_2} \rightarrow \mathrm{CO} + 2\mathrm{H_2O} \quad (R_{43})$$

$$\mathrm{CO} + \mathrm{H_2O} \leftrightarrow \mathrm{CO_2} + \mathrm{H_2} \quad (R_{44})$$

2.3. Reaction Kinetics Model

The evaporation volumetric rate is given by [12, 27, 28]:

$$R_1 = \begin{cases} A_1 \exp\left(-E_1 / R_u T_1\right) c_1 \rho_1 Y_M / M_M, & if\ T_1 < 373K \\ \dfrac{6(1-c_0)}{d_1} \dfrac{\left(\beta_{10}\left(T_0 - T_1\right) + \epsilon_m\, \sigma\left(T_m^4 - T_1^4\right)\right)}{H_{evap}}, & if\ T_1 \geq 373K \end{cases} \quad (1)$$

The kinetic constants are $A_1 = 5.56\times10^6$ and $E_1 = 8.79\times10^7\ Jkmol^{-1}$.

The reaction rates of biomass pyrolysis and tar cracking reaction can be written in the exponential form of the Arrhenius equation which is valid in most solid fuels [22, 27, 29, 30].

$$R_{21} = A_{21}\exp\left(-E_{21}/R_uT_1\right)c_1\rho_1Y_W/M_W \quad (2)$$

$$R_{22} = A_{22}\exp\left(-E_{22}/R_uT_1\right)c_1\rho_1Y_{Tar}/M_{Tar} \quad (3)$$

The values of the kinetic constants of the Eqs. R_{21} and R_{22} reactions are presented in Table **1**.

Table 1: Kinetics of the Devolatilization and Tar Cracking Reactions (R_{2i} in kmol $m^{-3}s^{-1}$ in all Reactions)

Reaction	A_{2i}	E_{2i} (J $kmol^{-1}$)	Ref.
R_{21}	4.38×10^9	1.527×10^8	[31]
R_{22}	4.28×10^6	1.08×10^8	[26]

The reaction rates for combustion and gasification of char are obtained through the unreacted shrinking core model, which considers two resistances: boundary layer diffusion and intrinsic chemical kinetics [25]. The reaction rates are given by:

$$R_{3i} = \begin{cases} \dfrac{6(1-c_0)}{d_1}\dfrac{p_{O_2}}{\dfrac{1}{k_{m1}}+\dfrac{1}{k_{31}}}, & if\ i = 1, O_2 \\ \dfrac{6(1-c_0)}{d_1}\dfrac{\rho_1 Y_i/M_i}{\dfrac{1}{k_{mi}}+\dfrac{1}{k_{3i}}}, & if\ i = 2, H_2O, i = 3, CO_2, i = 4, H_2 \end{cases} \quad (4)$$

The mass transfer coefficient, k_{mi}, is taken from [12]. The surface reaction takes the Arrhenius form as follows:

$$k_{3i} = A_{3i}\exp\left(-E_{3i}/R_uT_1\right) \quad (5)$$

The kinetic constants are given in Table **2**.

Table 2: Kinetics of the Heterogeneous Char Reactions (R_{3i} in kmol $m^{-3}s^{-1}$ in all reactions)

Reaction	A_{3i}	E_{3i} (J $kmol^{-1}$)	Ref.
R_{31}	4750	2×10^8	[12]
R_{32}	1×10^7	1.256×10^8	[12]
R_{33}	1×10^7	1.256×10^8	[12]
R_{34}	1×10^4	1.256×10^8	[12]

i=1(O_2), 2(H_2O), 3(CO_2), 4(H_2).

The reaction rates for homogeneous gas phase reactions used in the model are given in Table **3**. The finite-rate/eddy-dissipation model is taken to control the reaction rate. Both the Arrhenius and eddy-dissipation reaction rate are calculated. The net reaction rate is taken as the minimum of these two rates [32].

Table 3: Kinetics of the Homogenous Reactions (R_{4i} in kmol $m^{-3}s^{-1}$, C in kmol m^{-3} in all Reactions)

$R_{41} = A_{41}T_0^{\delta}\exp\left(-E_{41}/R_uT_0\right)C_{H2}^{\zeta}C_{O2}^{\eta}$					
ζ	η	δ	A_{41}	E_{41}(J $kmol^{-1}$)	Ref.
1	1	0	8.83×10^{11}	9.976×10^7	[12]
$R_{42} = A_{42}\exp\left(-E_{42}/R_uT_0\right)C_{CO}^{\zeta}C_{O2}^{\eta}C_{H2O}^{\theta}$					
ζ	η	θ	A_{42}	E_{42} (J $kmol^{-1}$)	Ref.
1	0.5	0.5	1.3×10^{11}	1.256×10^8	[12]
$R_{43} = A_{43}T_0^{\delta}\exp\left(-E_{43}/R_uT_0\right)C_{CH4}^{\zeta}C_{O2}^{\eta}$					
ζ	η	δ	A_{43}	E_{43} (J $kmol^{-1}$)	Ref.
1	1	0	2.552×10^{14}	9.304×10^8	[12]
$R_{44} = A_{44}\exp\left(-E_{44}/R_uT_0\right)C_{CO}C_{H2O}$					
A_{44}				E_{44} (J $kmol^{-1}$)	Ref.
1389				1.256×10^8	[12]

Table 4: Main Governing Equations

Mass Conservation
Gas phase:
$\frac{\partial(c_0\rho_0)}{\partial t} + \nabla\cdot(c_0\rho_0\boldsymbol{u}_0) = S_{0m}$
Solid phase:
$\frac{\partial(c_1\rho_1)}{\partial t} + \nabla\cdot(c_1\rho_1\boldsymbol{u}_1) = S_{1m}$
Momentum conservation
Gas phase:
$\frac{\partial(c_0\rho_0\boldsymbol{u}_0)}{\partial t} + \nabla\cdot(c_0\rho_0\boldsymbol{u}_0\otimes\boldsymbol{u}_0) = -c_0\nabla p + \nabla\cdot\bar{\bar{\tau}}_0 + c_0\rho_0\boldsymbol{g} + K_{10}(\boldsymbol{u}_1-\boldsymbol{u}_0) + \boldsymbol{S}_{0u}$
Solid phases:
$\frac{\partial(c_1\rho_1\boldsymbol{u}_1)}{\partial t} + \nabla\cdot(c_1\rho_1\boldsymbol{u}_1\otimes\boldsymbol{u}_1) = -c_1\nabla p - \nabla p_1 + \nabla\cdot\bar{\bar{\tau}}_1 + c_1\rho_1\boldsymbol{g} + K_{10}(\boldsymbol{u}_0-\boldsymbol{u}_1) + \boldsymbol{S}_{1u}$
Energy conservation
Gas phase:
$\frac{\partial(c_0\rho_0h_0)}{\partial t} + \nabla\cdot(c_0\rho_0\boldsymbol{u}_0h_0) = c_0\frac{\partial p_0}{\partial t} + \bar{\bar{\tau}}_0:\nabla\boldsymbol{u}_0 - \nabla\cdot\boldsymbol{q}_0 + Q_{10} + S_{0e}$
Solid phases:
$\frac{\partial(c_1\rho_1h_1)}{\partial t} + \nabla\cdot(c_1\rho_1\boldsymbol{u}_1h_1) = c_1\frac{\partial p_1}{\partial t} + \bar{\bar{\tau}}_1:\nabla\boldsymbol{u}_1 - \nabla\cdot\boldsymbol{q}_1 + Q_{01} + S_{1e}$
Species conservation
Gas phase:
$\frac{\partial(\rho_\alpha c_\alpha Y_{\alpha i})}{\partial t} + \nabla\cdot(\rho_\alpha c_\alpha\boldsymbol{u}_\alpha Y_{\alpha i}) = -\nabla\cdot c_\alpha\boldsymbol{J}_{\alpha i} + c_\alpha R_{\alpha i} + \mathcal{R}_{\alpha i} + S_{\alpha is}$, Where, $\boldsymbol{J}_{\alpha i} = -\left(\rho_\alpha D_{im} + \frac{\mu_{t\alpha}}{Sc_{t\alpha}}\right)\nabla Y_{\alpha i}$
$k-\varepsilon$ mixture turbulence equation
$\frac{\partial}{\partial t}(\rho_m k) + \nabla\cdot(\rho_m k\boldsymbol{u_m}) = \nabla\cdot\left(\left(\mu_m + \frac{\mu_{tm}}{\sigma_k}\right)\nabla k\right) + G_{km} - \rho_m\varepsilon + \Pi_{km}$
$\frac{\partial}{\partial t}(\rho_m\varepsilon) + \nabla\cdot(\rho_m\varepsilon\boldsymbol{u_m}) = \nabla\cdot\left(\left(\mu_m + \frac{\mu_{tm}}{\sigma_\varepsilon}\right)\nabla\varepsilon\right) + \frac{\varepsilon}{k}(C_{1\varepsilon}G_{km} - C_{2\varepsilon}\rho_m\varepsilon) + \Pi_{\varepsilon m}$
P-1 radiation model [32, 33]
$\nabla\cdot(\Gamma\nabla G) - \sigma_a G + 4\pi\sigma_a I_b = 0$ $\nabla\cdot\boldsymbol{q}_r = \sigma_a(4\pi I_b - G)$

3. CFD MODELING

3.1. Flow Equations

CFD model is based on the Euler-Euler multiphase approach using closures from the KTGF for the solid phase. Particles in the solid phase are in enduring contact, making the frictional stresses the dominant mechanism for momentum transfer. The P-1 radiation model was used in this study because it is suitable for applications where the optical thickness is large. The weighted sum of gray gases model (WSGGM) for the radiative properties of the gases was applied. To take into account bed particles, an equivalent solid phase absorption coefficient was assumed.

Details of the computational flow equations are shown in Table **4**. A few constitutive equations and exchange co-efficients used in the model are shown in Table **5**. The reaction kinetics equations were also incorporated into the computational flow equations.

Table 5: A Summary of the Constitutive Equations and Exchange Coefficients

Stress Tensor
Gas phase:
$\bar{\tau}_0 = c_0\mu_0(\nabla \boldsymbol{u}_0 + \nabla \boldsymbol{u}_0^T) + c_0\left(\lambda_0 - \frac{2}{3}\mu_0\right)\nabla \cdot \boldsymbol{u}_0\bar{\boldsymbol{I}}$
Solid phase:
$\bar{\tau}_1 = \begin{cases} c_1\mu_1(\nabla \boldsymbol{u}_1 + \nabla \boldsymbol{u}_1^T) + c_1\left(\lambda_1 - \frac{2}{3}\mu_1\right)\nabla \cdot \boldsymbol{u}_1\bar{\boldsymbol{I}}, & if\ c_1 < c_{1,min} \\ \mu_{1,fr}(\nabla \boldsymbol{u}_1 + \nabla \boldsymbol{u}_1^T), & if\ c_1 \geq c_{1,min} \end{cases}$
Gas-solid interphase momentum exchange coefficient [34]
$K_{10} = \psi K_{10}^1 + (1-\psi)K_{10}^2$, where $\psi = \frac{1}{2} + \frac{\tan^{-1}(262.5[c_1 - 0.2])}{\pi}$
$K_{10}^1 = 150\frac{c_1(1-c_0)\mu_0}{c_0 d_1^2} + 1.75\frac{\rho_0 c_1 \lvert\boldsymbol{u}_1 - \boldsymbol{u}_0\rvert}{d_1}$
$K_{10}^2 = \frac{3}{4}\frac{\rho_0 c_1 c_0 \lvert\boldsymbol{u}_1 - \boldsymbol{u}_0\rvert}{d_1} {c_0}^{-2.65}\left\{\frac{24}{c_0 \mathrm{Re}_1}(1 + 0.15[c_0\mathrm{Re}_1]^{0.687})\right\}$
Solid pressure [32, 35]
$p_1 = \begin{cases} c_1\rho_1\theta_1 + 2\rho_1(1+e_{11}){c_1}^2 g_0\theta_1, & if\ c_1 < c_{1,min} \\ c_1 A(c_1 - c_{1,min})^n, & if\ c_1 \geq c_{1,min} \end{cases}$
Heat transfer coefficient between gas and solid phases [36]
$h_{10}A_i = \frac{6\kappa_0 c_1 c_0 \mathrm{Nu}_1}{d_1^2}$
$\mathrm{Nu}_\alpha = (7 - 10c_0 + 5c_0^2)(1 + 0.7\mathrm{Re}_1^{0.2}\mathrm{Pr}^{1/3}) + (1.33 - 2.4c_0 + 1.2c_0^2)\mathrm{Re}_1^{0.7}\mathrm{Pr}^{1/3}$

3.2. CFD Modeling Method and Parameters

An unsteady two-dimensional axisymmetric CFD simulation was performed using the finite volume method implemented in FLUENT. The computational model was based on an updraft fixed bed gasifier experimented on by Mandl *et al*. [12], whose characteristics are shown in Table **6** and Table **7**.

Table 6: Updraft Fixed Bed Gasifier Model Characteristics Based on Mandl *et al*. [12]

Gasifier Geometry	
Column diameter (mm), D	125
Height of gasifier (mm), H	600
Bed height (mm), H_b	420

A total of 6 cases were simulated, as shown in Table **8**. For all cases, a uniform mass flow inlet boundary condition, a constant outlet pressure condition and the same initial conditions were applied. Inlet air composition remained constant at $X_{O2} = 0.21$, $X_{N2} = 0.785$ and $X_{H_2O} = 0.005$ and in let temperature (gas and solid phases) at 300 K. The fluid was assumed to obey the no-slip boundary condition on the inner wall of the reactor. In addition, walls were assumed adiabatic.

Table 7: Characterization of the Biomass used by Mandl *et al*. [12]

Composition (wt.% dry basis)	
Moisture	6.0 (wet basis)
C	48.7
H	6.2
N	0.06
Ash	0.4
Particle diameter (mm), d_1	10.1
Net calorific value (kJ/kg wet basis.)	17060

The pressure-velocity coupling method used for the transient simulations was the phase coupled SIMPLE. Turbulence modeling was done with with $k-\varepsilon$ mixture turbulence model, depending on the case. Second order discretization was used during transient

Table 8: Operating Parameters for the Simulation of the Gasifier for Different Reynolds Numbers (Re) and Viscous Models

Case	1	2	3	4	5	6
Re	1200	480	2500	4030	2400	2400
Mass flow rate of gas (kg/h)	2.1	0.84	4.37	7.06	4.2	4.2
Mass flow rate of solid (kg/h)	1.25	0.5	2.6	4.2	3.5	3.5
Viscous model	laminar	laminar	turbulent	turbulent	laminar	turbulent
Equivalence ratio, ϕ	0.28	0.28	0.28	0.28	0.2	0.2

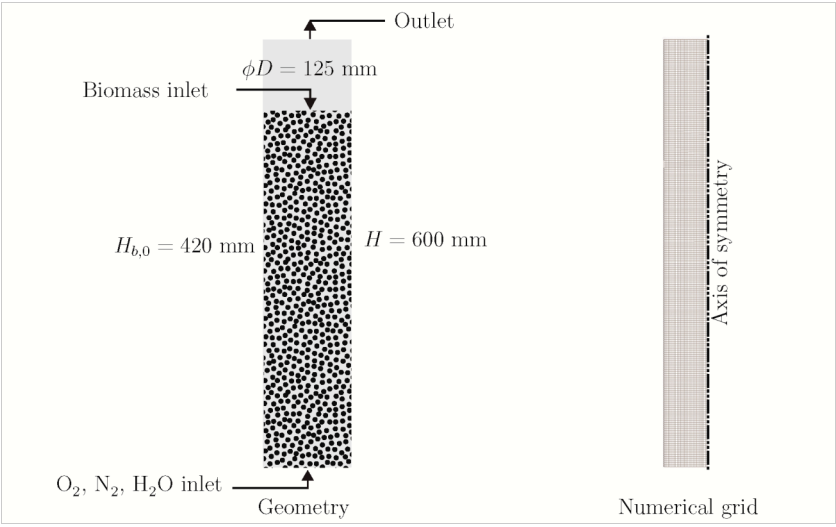

Figure 1: Geometry of the fixed bed reactor and numerical grid used.

simulations for pressure, momentum, turbulent kinetic energy, turbulent dissipation rate, species (gas and solid) and energy variables.

The computational domain is shown in Figure **1**, including boundary conditions. The meshing was performed with ANSYS Meshing. It was structured quadrilateral elements. A summary of the most important mesh metrics is shown in Table **9**.

Table 9: Mesh Metrics

Metric	Value
Number of Elements	6000
Number of Nodes	6293
Cell squish (Maximum)	8e-6
Aspect ratio (Maximum)	1.75

In order to verify that the CFD results were independent of the mesh grid, cold-flow simulations with three different mesh grids (15 × 100, 30 × 200, 60 × 400) were performed. Figure **2** shows the pressure drop values. It is observed that the predicted pressure drops are almost the same. Compared with coarse mesh, the fine (60 × 400) and medium (30 × 200) meshes can produce similar pressure drop

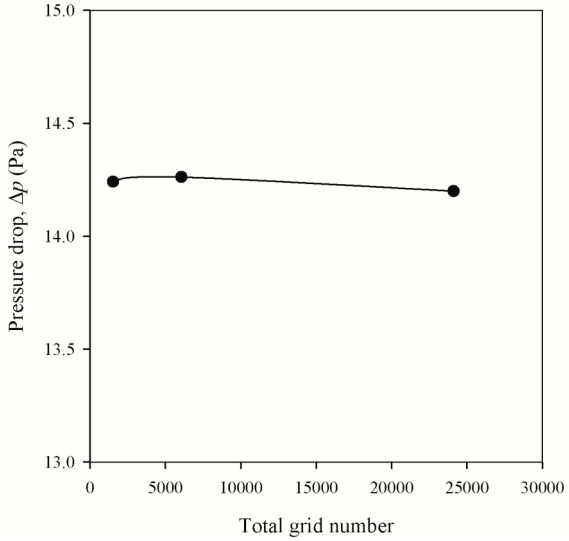

Figure 2: Pressure drop at various mesh resolutions.

profiles along the reactor. Therefore, the mesh size of 30 × 200 was selected and applied to the remaining simulations.

4. RESULTS AND DISCUSSION

In this section, numerical results of the cases mentioned above are presented. For all cases, the solution is obtained when the quasi-steady state is reached.

4.1. Comparison of Case 5 with Data of Mandl *et al.*

4.1.1. Temperature Distribution

The flow is almost certainly laminar in the spaces between the particles. Figure **3**(**a**) compares centerline temperature distribution along the reactor axis predicted by numerical simulations with respect to experimental results. It is observed that the maximum temperature which has been found is close to that measured experimentally, around 1473 K. Moreover, in Figure **3**(**b**) we see the normalized centerline temperature, showing three different slopes attributed to three distinct zones existing within the reactor. First, combustion zone, where the temperature of the gasifier increases rapidly and reaches a maximum due to a large amount of heat released by combustion (reaction R_{31}). R_{31} reaction occurs in a layer near the reactor inlet. Second, a gasification zone, where the temperature gradually descends along the height of the reactor since the reactions R_{32}, R_{33}, and R_{34} absorb heat. Finally, a pyrolysis zone, where endothermic reaction R_{21} occurs, leading to a decrease in temperature. Near the fuel inlet the lowest temperature occurs (x/H_b=1) due to heat absorption by drying (R_1 reaction).

Figure **4** shows the contours of gas temperature and solid phase in the reactor. Predicted temperatures

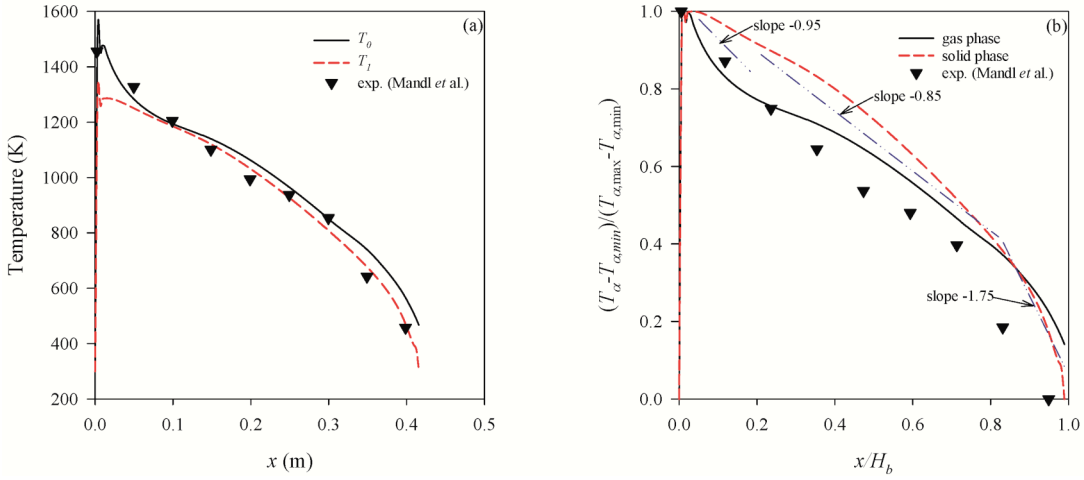

Figure 3: Axial profiles of solid and gas phase temperatures; bed height constant at 0.42 m; position of grate at x = 0 m.; case 5: (**a**) predicted and experimental temperatures; (**b**) normalized temperatures.

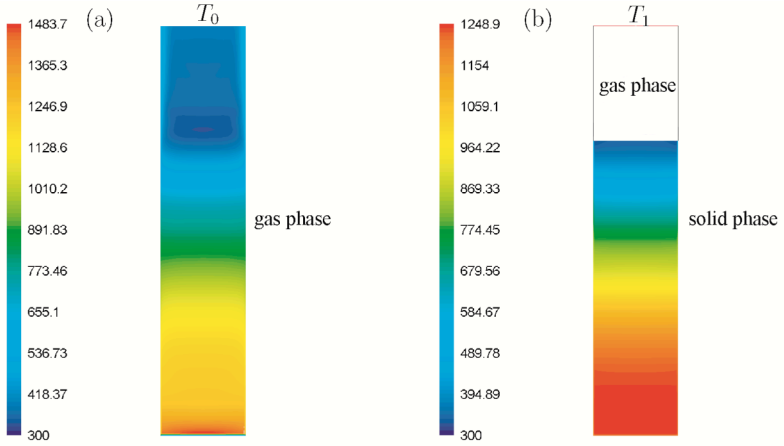

Figure 4: Contours of solid and gas phase temperatures (Temperature in Kelvin); bed height constant at 0.42 m; position of grate at x = 0 m.; case 5: (**a**) gas phase; (**b**) solid phase.

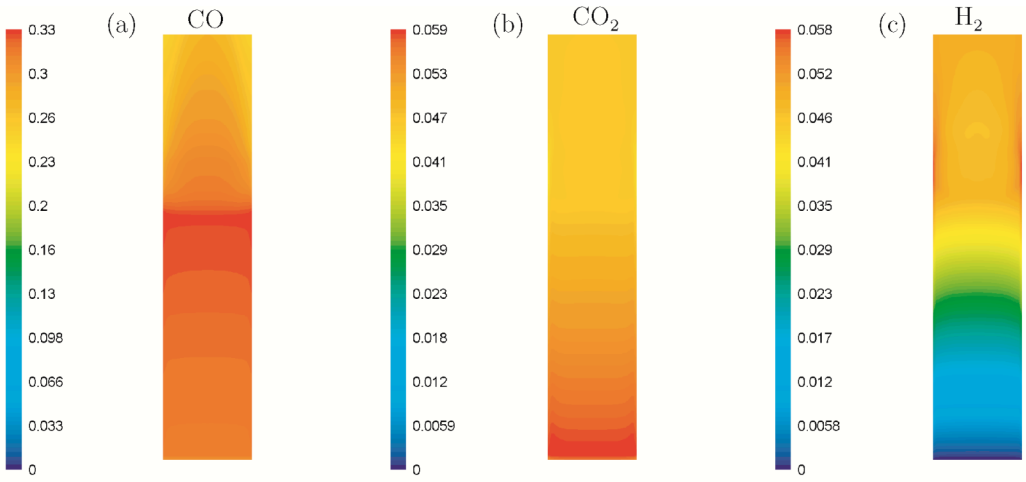

Figure 5: Contours of predicted mole fraction of species (dry basis); case 5: (**a**) CO; (**b**) CO_2; (**c**) H_2.

agree with experimental values, especially in the zone of combustion, pyrolysis and the thin layer of drying. The differences observed in the gasification zone should be due to chemical kinetics used.

4.1.2. Component Distribution

Figure **5** shows the contours of mole fraction on dry basis of the three major chemical species in the reactor, namely, CO, CO_2 and H_2. The CO concentration in the gasifier is higher because it can be formed not only on the combustion reaction (R_{31}), but also in the R_{21}, R_{32}, and R_{33} reactions. The mole fraction of CO decreases in the drying layer since the R_{44} reaction. Consequently, the mole fraction of CO_2 and H_2 increases. Tar appears as a result of pyrolysis and its concentration is influenced by the stoichiometry of reaction R_{21}. Heterogeneous reaction rates along the reactor axis are shown in Figure **6**. Figure **7** shows the compositions on the dry basis of CO, CO_2, CH_4, Tar, and H_2 to the reactor outlet and they are compared with the experimental data. It is observed that gas compositions are in good agreement with experimental values.

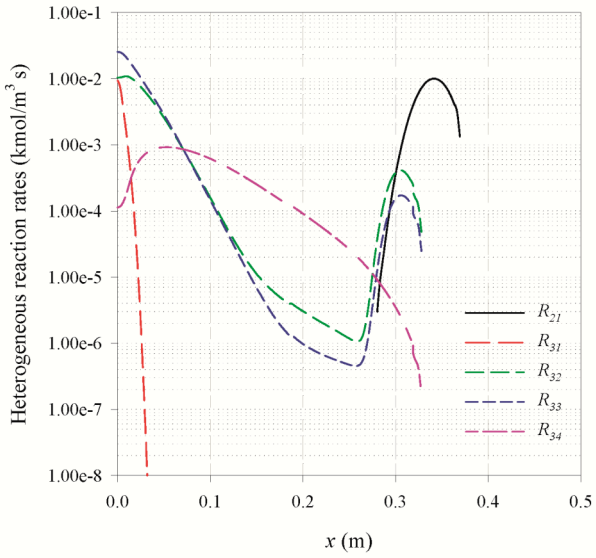

Figure 6: Axial profiles of heterogeneous reaction rates; bed height constant at 0.42m; position of grate at x=0m; case 5.

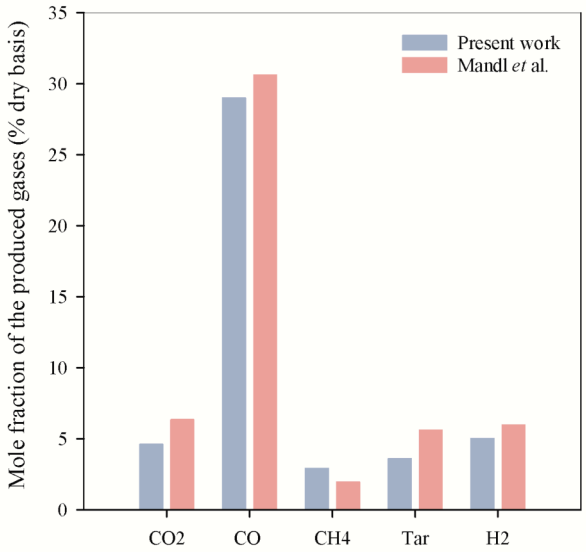

Figure 7: Comparison between models predictions and experimental measurements; case 5.

4.2. Effect of Viscous Models in the Biomass Gasification

Figure **8** shows the numerical results for the net calorific value of producer gas during gasification for different models viscous. The results show that in cases where the laminar model was used, the predicted net calorific value agrees with experimental values. Conversely, the cases where the $k-\varepsilon$ mixture

model was used, the gasification process tends to stop with increasing Reynolds number. It was determined that this behavior is due to the spatial movement of the combustion zone in time. Accordingly, a decrease in temperature occurs to the point of not being able to sustain the series of endothermic reactions.

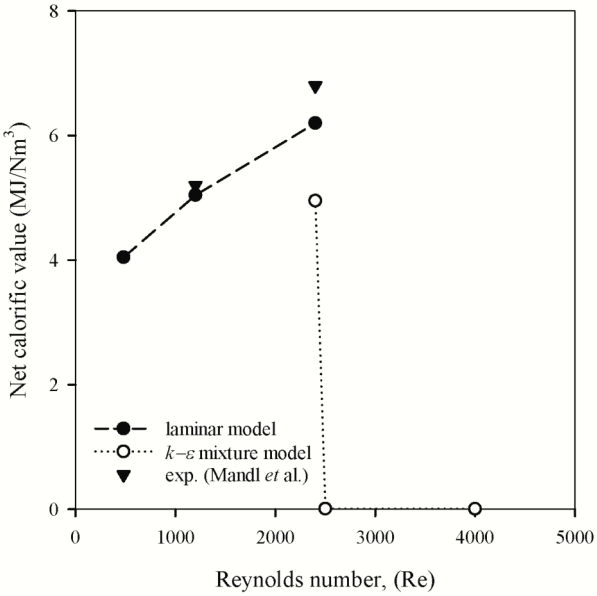

Figure 8: Net Calorific Value of producer gas.

CONCLUSIONS

A 2D axisymmetric CFD model was created within the commercial CFD code ANSYS FLUENT to simulate biomass gasification in updraft fixed bed reactors. The model was used to investigate the influence of viscous model in the biomass gasification in an updraft fixed bed reactor. Numerical results were validated with experimental data obtained by Mandl *et al*.

The maximum temperature obtained by simulation was close to that obtained experimentally by Mandl *et al*. The temperatures obtained by the simulations within the gasifier were in good agreement with experimental measurements. The differences observed in the gasification zone are related to chemical kinetics used by the model.

Inspections of the 2D contours indicate that the flow is closely one-dimensional. The results are essentially the same as Mandl's 1D model. The extension from 1D to 2D has added no new essential physics. However, the developed model is easily extended to deal with 3D geometries, which can be used in gasifier design, analysis, and optimization.

The higher concentration obtained was CO because it is both produced by the combustion reaction as well as gasification reactions. Tar appears only as a product of pyrolysis reaction and its concentration is determined by the stoichiometry. The mole fractions of CO, CO_2, CH_4, Tar, and H_2 at the reactor outlet were in good agreement with the experimental measurements.

The laminar model and the $k-\varepsilon$ mixture model were used. The viscous model has a significant effect on biomass gasification. Predicted values with the laminar model were agreed with experimental values. In contrast, when the $k-\varepsilon$ mixture model was used, it is observed that not occurs biomass gasification.

The work carried out in this study provides new challenges for research on biomass gasification. Further improvements in the model can be achieved by considering a more detailed chemical kinetics for both pyrolysis and gasification.

NOMENCLATURE

A_i Interfacial area, m^{-1}

C Molar concentration, kg m^{-3}

C Volume fraction, m^3m^{-3}

$c_{1,\,min}$ Critical value for the solid volume fraction

$c_{1,\,max}$ Maximum volume fraction for the solid phase

D Mass diffusion coefficient, m^2s^{-1}

D_h Hydraulic diameter, m

d_1 Particle diameter, m

d_{1e} Equivalent diameter, m

e_{11} Coefficient of restitution

E Activation energy, kJ mol^{-1}

F Linear-anisotropic phase function coefficient

g_0 Radial distribution function

g Acceleration of gravity, m s^{-2}

G Incident radiation, W m^{-2}

h Specific enthalpy, J kg^{-1}

H_{evap} Heat of vaporization of water, 40.7×10^6 J $kmol^{-1}$

$\bar{I}$ Identity tensor

I_b Radiation intensity, W sr−1

I_{2D} Second invariant of the deviatoric stress tensor

J Diffusion flux discusion, kg m^{-2} s^{-1}

K Interphase momentum exchange coefficient, kg m^{-3} s^{-1}

k Turbulent kinetic energy, m^2 s^{-2}

k_m Mass transfer coefficient, m s^{-1}

M Molecular mass, kg $kmol^{-1}$

Nu Nusselt number

Pr Prandtlnumber

p Pressure, Pa

p_1 Solid pressure, Pa

q_r Radiative flux density, W m^{-2}

Q Volumetric rate of energy transfer between phases, W m^{-3}

R Heterogeneous reaction rate, kmol m^{-3} s^{-1}

Re Reynolds number

R Reaction rate, net rate of production of homogeneous species, kmol $m^{-3}s^{-1}$

R_u Universal gas constant, 8314 JK^{-1} $kmol^{-1}$

Sc Schmidt number

Sh Sherwood number

S, S Source of a transported property per unit of volume unit of transported property

t Time, s

T Temperature, K

u, u Velocity, m s^{-1}

V Volume, m^3

X Mole fraction, kmol $kmol^{-1}$

Y Mass fraction, kg kg^{-1}

GREEK SYMBOLS

β Stoichiometric coefficient, heat transfer coefficient, J m^{-2} s^{-1} K^{-1}

γ Stoichiometric coefficient

Γ Diffusion, m

κ Thermal conductivity, W m^{-1} K^{-1}

$\in_m$ Emissivity

ε Turbulent dissipation rate, m^2 s^{-3}

θ Granular temperature, m^2 s^{-2}

λ Bulk viscosity, Pa-s

μ Dynamic viscosity, shear viscosity, Pa-s

μ_t Turbulent viscosity, Pa-s

ϕ Sphericity

φ Angle of internal friction, deg

ρ Density, kg m^{-3}

$\hat{\rho}$ Effective density, kg m^{-3}

σ Stefan–Boltzmann constant, $5.670373(21)\times10^{-8}$ W m^{-2} K^{-4}

σ_1 Scattering coefficient, m^{-1}

σ_a Absorption coefficient, m^{-1}

τ Stress tensor, Pa

ζ Permeability, m^2

SUBSCRIPTS

αe Energy equation, phase α

αi ^{i}th species transport equation, phase α

αm Continuity equation, phase α

αu Momentum equation, phase α

α Phase index (0=gas, 1=solid)

col Collisional component of viscosity

fr Frictional component of viscosity

kin Kinetic component of viscosity

m Mixture, mass

t Turbulent

0 Gas phase

1 Solid phase

1W Solid specie: wood

ACKNOWLEDGMENTS

The research reported on this paper was supported by CONICYT-PCHA/*MagísterNacional*/2013-22130285 grant for Master's studies in Chile. The authors would like to acknowledge the Universidad de Chile, which through its Center for Mathematical Modeling (CMM) has provided the supercomputing infrastructure of the NLHPC (ECM-02) and the Master's Program of the *Departamento de Ingeniería Mecánica* for its financial support.

REFERENCES

[1] Desrosiers RE and Lin RJ. A moving-boundary model of biomass pyrolysis, Sol. Energy 1984; 33: 187-196. http://dx.doi.org/10.1016/0038-092X(84)90237-8

[2] Sharma AK. Equilibrium modeling of global reduction reactions for a downdraft (biomass) gasifier. Energy Convers Manag 2008; 49: 832-842. http://dx.doi.org/10.1016/j.enconman.2007.06.025

[3] Kayal TK, Chakravarty M and Biswas GK. Mathematical modelling of continuous updraft gasification of bundled jute stick -- a low ash content woody biomass. Bioresour Technol 1994; 49: 61-73. http://dx.doi.org/10.1016/0960-8524(94)90174-0

[4] Mikulandrić R, Lončar D, Böhning D, Böhme R and Beckmann M. Artificial neural network modelling approach for a biomass gasification process in fixed bed gasifiers. Energy Convers Manag 2014. http://dx.doi.org/10.1016/j.enconman.2014.03.036

[5] Mahmoudi AH, Hoffmann F and Peters B. Detailed numerical modeling of pyrolysis in a heterogeneous packed bed using XDEM. J Anal Appl Pyrolysis 2014; 106: 9-20. http://dx.doi.org/10.1016/j.jaap.2013.12.001

[6] Fletcher DF, Haynes BS, Christo FC and Joseph SD. A CFD based combustion model of an entrained flow biomass gasifier. Appl Math Model 2000; 24: 165-182. http://dx.doi.org/10.1016/S0307-904X(99)00025-6

[7] Ismail TM and El-Salam MA. Numerical and experimental studies on updraft gasifier HTAG. Renew Energy 2015; 78: 484-497. http://dx.doi.org/10.1016/j.renene.2015.01.032

[8] Gómez-Barea A and Leckner B. Modeling of biomass gasification in fluidized bed. Prog Energy Combust Sci 2010; 36: 444-509. http://dx.doi.org/10.1016/j.pecs.2009.12.002

[9] Mendes A, Dollet A, Ablitzer C, Perrais C and Flamant G. Numerical simulation of reactive transfers in spouted beds at high temperature: Application to coal gasification. J Anal Appl Pyrolysis 2008; 82: 117-128. http://dx.doi.org/10.1016/j.jaap.2008.02.001

[10] Salam PA and Bhattacharya SC. A comparative study of charcoal gasification in two types of spouted bed reactors. Energy 2006; 31: 228-243. http://dx.doi.org/10.1016/j.energy.2005.01.004

[11] Xia Z, Fan Y, Wang T, Guo X and Chen C. A TFM-KTGF jetting fluidized bed coal gasification model and its validations with data of a bench-scale gasifier. Chem Eng Sci 2015; 131: 12-21. http://dx.doi.org/10.1016/j.ces.2015.03.017

[12] Mandl C, Obernberger I and Biedermann F. Modelling of an updraft fixed-bed gasifier operated with softwood pellets. Fuel 2010; 89: 3795-3806. http://dx.doi.org/10.1016/j.fuel.2010.07.014

[13] Umeki K, Namioka T and Yoshikawa K. Analysis of an updraft biomass gasifier with high temperature steam using a numerical model. Appl Energy 2012; 90: 38-45. http://dx.doi.org/10.1016/j.apenergy.2010.12.058

[14] Lucas C. High temperature air/steam gasification of biomass in an updraft fixed bed batch type gasifier. Royal Institute of Technology 2005.

[15] Yang W, Ponzio A, Lucas C and Blasiak W. Performance analysis of a fixed-bed biomass gasifier using high-temperature air. Fuel Process Technol 2006; 87: 235-245. doi:10.1016/j.fuproc.2005.08.004. http://dx.doi.org/10.1016/j.fuproc.2005.08.004

[16] Di Blasi C, Signorelli G and Portoricco G. Countercurrent Fixed-Bed Gasification of Biomass at Laboratory Scale. Ind Eng Chem 1999; 38: 2571-2581. http://dx.doi.org/10.1021/ie980753i

[17] Blasi CD. Dynamic behaviour of stratified downdraft gasifiers. In Chem Eng Sci 2000: 2931-2944. http://dx.doi.org/10.1016/S0009-2509(99)00562-X

[18] Tinaut FV, Melgar A, Pérez JF and Horrillo A. Effect of biomass particle size and air superficial velocity on the gasification process in a downdraft fixed bed gasifier. An experimental and modelling study. Fuel Process Technol 2008; 89: 1076-1089. http://dx.doi.org/10.1016/j.fuproc.2008.04.010

[19] Gerun L, Paraschiv M, Vîjeu R, Bellettre J, Tazerout M, Gøbel B, et al. Numerical investigation of the partial oxidation in a two-stage downdraft gasifier. Fuel 2008; 87: 1383-1393. http://dx.doi.org/10.1016/j.fuel.2007.07.009

[20] Wu Y, Zhang Q, Yang W and Blasiak W. Two-Dimensional Computational Fluid Dynamics Simulation of Biomass Gasification in a Downdraft Fixed-Bed Gasifier with Highly Preheated Air and Steam. Energy and Fuels 2013; 27: 3274-3282. http://dx.doi.org/10.1021/ef4003704

[21] Manchasing C, Kuchonthara P, Chalermsinsuwan B and Piumsomboon P. Experiment and computational fluid dynamics simulation of in-depth system hydrodynamics in dual-bed gasifier. Int J Hydrogen Energy 2013; 38: 10417-10430. http://dx.doi.org/10.1016/j.ijhydene.2013.06.033

[22] Kær SK. Straw combustion on slow-moving grates - A comparison of model predictions with experimental data. Biomass and Bioenergy 2005; 28: 307-320. http://dx.doi.org/10.1016/j.biombioe.2004.08.017

[23] de Souza-Santos ML. Solid Fuels Combustion and Gasification: Modeling, Simulation and Equipment Operations Second Edition. CRC Press 2010. https://books.google.com/books?id=8_rLBQAAQBAJ&pgis=1 (accessed September 9, 2015). http://dx.doi.org/10.1201/9781420047509

[24] Thunman H, Niklasson F, Johnsson F and Leckner B. Composition of volatile gases and thermochemical properties of wood for modeling of fixed or fluidized beds. Energy and Fuels 2001; 15: 1488-1497. http://dx.doi.org/10.1021/ef010097q

[25] Di Blasi C. Modeling wood gasification in a countercurrent fixed-bed reactor. AIChE J 2004; 50: 2306-2319. http://dx.doi.org/10.1002/aic.10189

[26] Rath J and Staudinger G. Cracking reactions of tar from pyrolysis of spruce wood. Fuel 2001; 80: 1379-1389. http://dx.doi.org/10.1016/S0016-2361(01)00016-3

[27] Yang YB, Yamauchi H, Nasserzadeh V and Swithenbank J. Effects of fuel devolatilisation on the combustion of wood chips and incineration of simulated municipal solid wastes in a packed bed. Fuel 2003; 82: 2205-2221. http://dx.doi.org/10.1016/S0016-2361(03)00145-5

[28] Bin Yang Y, Ryu C, Sharifi VN and Swithenbank J. Effect of Model and Operating Parameters on Air Gasification of Char. Energy and Fuels 2006; 20: 1698-1708. http://dx.doi.org/10.1021/ef060036y

[29] Di Blasi C. Modeling chemical and physical processes of wood and biomass pyrolysis. Prog Energy Combust Sci 2008; 34: 47-90. http://dx.doi.org/10.1016/j.pecs.2006.12.001

[30] Cao Y, Wang Y, Riley JT and Pan WP. A novel biomass air gasification process for producing tar-free higher heating value fuel gas. Fuel Process Technol 2006; 87: 343-353. http://dx.doi.org/10.1016/j.fuproc.2005.10.003

[31] Di Blasi C, Signorelli G, Di Russo C and Rea G. Product Distribution from Pyrolysis of Wood and Agricultural Residues. Ind Eng Chem Res 1999; 38: 2216-2224. http://dx.doi.org/10.1021/ie980711u

[32] ANSYS I. ANSYS FLUENT Theory Guide. Release 2009; 12.

[33] Krishnamoorthy G, Rawat R and Smith PJ. Parallelization of the P-1 Radiation Model. Numer Heat Transf Part B Fundam 2007.

[34] Huilin L and Gidaspow D. Hydrodynamics of binary fluidization in a riser: CFD simulation using two granular temperatures. Chem Eng Sci 2003; 58: 3777-3792. http://dx.doi.org/10.1016/S0009-2509(03)00238-0

[35] Syamlal M, Rogers W and O`Brien TJ. MFIX documentation theory guide 1993. http://dx.doi.org/10.2172/10145548

[36] Gunn DJ. Transfer of heat or mass to particles in fixed and fluidised beds. Int J Heat Mass Transf 1978; 21: 467-476. http://dx.doi.org/10.1016/0017-9310(78)90080-7

Received on 13-07-2016 Accepted on 19-07-2016 Published on 13-12-2016

DOI: http://dx.doi.org/10.15377/2409-5826.2016.03.02.01